Journal of Inorganic and Organometallic Polymers and Materials (2021) 31:319–330
https://doi.org/10.1007/s10904-020-01784-3

Effective Reduction of Cr(VI) and Organic Dyes Using Pd NPs/Fe_3O_4@nanocellulose as a Recoverable Catalyst in Aqueous Media

Elmira Kalantari[1] · Mohammad A. Khalilzadeh[1] · Daryoush Zareyee[1]

Received: 4 June 2020 / Accepted: 9 October 2020 / Published online: 18 October 2020

Abstract
In this work, the extract of the roots plant of *Chelidonium majus* (greater celandine) was used to synthesize a magnetically reusable Pd nanoparticles supported by Fe_3O_4@nanocellulose through a green synthesis method. The Pd NPs/Fe_3O_4@nanocellulose catalyst as an impressive catalyst was prepared via reduction of Pd^{2+} ions using *Chelidonium majus* extract as bioreductant agent. The synthesized Pd NPs/Fe_3O_4@nanocellulose was characterized using vibrating sample magnetometer, field emission scanning electron microscopy, transmission electron microscopy, X-ray diffraction analysis, energy-dispersive X-ray spectroscopy, fourier transform infrared spectroscopy and thermogravimetric analysis techniques. This heterogeneous catalyst represented excellent activity for full degradation of Cr(VI) in the presence of formic acid at 50 °C, and reduction of methylene blue, methyl orange, rhodamine B and congo red in the presence of $NaBH_4$ as a reducing agent at room temperature. The synthesized catalyst was also reused four times for the reduction reactions without significant activity loss.

Keywords Catalyst · Nanocellulose · Reduction · Organic dyes · Degradation

1 Introduction

Recently, chromium pollution, particularly by hexavalent chromium Cr(VI), has become one of the biggest hectic problems of environment for the scientists. The hexavalent chromium is about 500 times more toxic than that of the trivalent form [1] for plants, microorganism, animals and humans [2, 3]. It has been reported that the Cr(VI) content should not exceed 0.05 mg L^{-1} in the waste water [4]. The excessive level of chromium metals has also caused damage to kidney and liver [5, 6]. World health organization has recognized that the Cr(VI) is even cancerous [7]. Reciprocally, trivalent chromium Cr(III) is less toxic and less mobile in nature. For animal and human, it has been shown that small amount of Cr(III) is required for metabolism of sugar, carbohydrate and lipid [8].

There are various conventional methods to eliminate organic compounds from the industrial wastewaters, such as prevalent chemical oxidation, adsorption, biodegradation, flocculation-coagulation, electro-coagulation. However, there has been no impressive way in attaining whole removal of these organic compounds [9]. Recently, some practical and economical methods have been developed to reduce Cr(VI) to Cr(III) [10–12]. For instance, Daneshvar et al. [13] used soya cake as the reducing agent and observed a high efficiency in reduction of Cr(VI) to Cr(III). Dandapat et al. [14] reduced Cr(VI) to Cr(III) in the presence of formic acid using relatively thick Pd NP-incorporated mesoporous γ-Al_2O_3 films as a catalyst. These studies suggest that Pd NPs/Fe_3O_4@nanocellulose catalyst could be applied as an efficient catalyst for environmental amendment of Cr(VI) and organic dyes. More importantly, separation and reuse of the costly Pd NPs are crucial due to the rarity of metal Pd and the further possible environmental contamination risk of colloidal Pd NPs in aqueous media or soil. Therefore, for practical environmental remediation applications, it is necessary to develop various supporting materials that are able to efficiently immobilize Pd NPs and retain their catalytic activity.

Cellulose is considered as one of the most plenty organic polymers in nature [15], and has been applied as a precursor of functional materials [16]. Also, it has been reported that cellulose is the best support material for the heterogeneous catalysts due to its good mechanical properties, large surface area, biodegradability, and renewable properties [17].

✉ Mohammad A. Khalilzadeh
mkhalil3@ncsu.edu

[1] Department of Chemistry, Qaemshahr Branch, Islamic Azad University, Qaemshahr, Iran

Cellulose contains strong inter- and intra-molecular hydrogen bonds owing to abundant of hydroxyl groups, which can be a significant factor to anchor metal oxide nanoparticles such as Fe_3O_4. For instance, Jiao et al. [18] immobilized Fe_3O_4 nanoparticles onto cellulose aerogel to prepare Fenton-like catalyst by a hydrothermal method, which demonstrated a superior degradation rate for rhodamine B than pure Fe_3O_4 nanoparticles. In addition, magnetic nanoparticles (MNPs) have been effectively applied in countless fields such as drug delivery [19], cancer treatment [20] and facility of catalyst separation. Among the various MNPs, iron oxide MNPs (Fe_3O_4 MNPs) have been widely used in inorganic and organic transformations due to their inimitable properties such as low cost, high special surface area good electronic characteristics, and magnetic separability [21–25].

In recent decades, plant extracts for metal NPs synthesis have widely been used by many researchers. There are many chemical methods used for metal NPs synthesis because of their high production efficiency [26], and their swift reaction time [27]. However, those chemical methods have some disadvantages such as creating environmental pollution due to using toxic solvents and reducing agent [28] and high price of the process. The most important principle in the green synthesis approaches is that the phytochemicals, presenting in the different parts of the plant, are both natural reducing and nanoparticles stabilizing [29]. It has been shown that quick synthesis of highly stabilized NPs from the plant extracts could be an impressive approach for reducing and stabilizing of NPs [30].

Herein, we have demonstrated a simple green synthesis method for producing the Pd NPs/Fe_3O_4@nanocellulose catalyst using roots of *Chelidonium majus* aqueous extract as a reductant agent to reduce Pd (II) to Pd nanoparticles. The synthesized catalyst was assessed by degradation of Cr(VI) in the presence of formic acid (HCOOH) and reduction of methylene blue (MB), methyl orange (MO), rhodamine B (RhB) and congo red (CR) in the presence of $NaBH_4$. The schematic illustration of NOs synthesis using the plant extracts is shown in Fig. 1. The plant extracts play a dual task by acting as both stabilizing and reducing agents in synthesis of nanoparticles [31]. In addition the plant extracts facilitate metal atoms nucleation and growth to form nanoparticles.

2 Materials and Methods

Chelidonium majus plant was collected from nearby Bandargaz, Golestan, Iran for green synthesis of nanoparticles of palladium. All of the chemical compounds were obtained from Aldrich and Merck companies and directly used for the experiments. Double-beam ultraviolet–visible spectroscopy (UV–Vis) was carried out using a Hitachi, U-2900 to ensure the reduction of Cr(VI), MB, MO, RhB, CR and to investigate the plant extract. Fourier transform infrared (FT-IR) spectra were obtained on a Perkin Elmer spectrophotometer using pressed KBr pellets. Elemental mapping analysis was conducted using energy dispersive X-ray spectroscopy (EDS) to confirm the elements dispensation in the synthesized catalyst. The chemical composition of the synthesized catalyst was also studied by EDS. Transmission electron microscopy (TEM) and field emission scanning electron microscopy (FE-SEM) were utilized to identify morphology and size of the synthesized catalyst particles using ZEISS EM10C-100 kV system and Cam scan Mv2300 system, respectively. X-ray Diffraction (XRD) analysis was done using a Philips model X' Pert Pro diffractometer employing Cu K_α radiation ($\lambda = 1.5418$ Å) in the 2θ range of 20°–90° to determine structure of the catalyst. Thermogravimetric analysis (TGA) was conducted using STA 1500 Rheometric Scientific system. Vibrating sample magnetometer (VSM) measurement was also achieved by using a Quantum Design MPMS XL at room temperature.

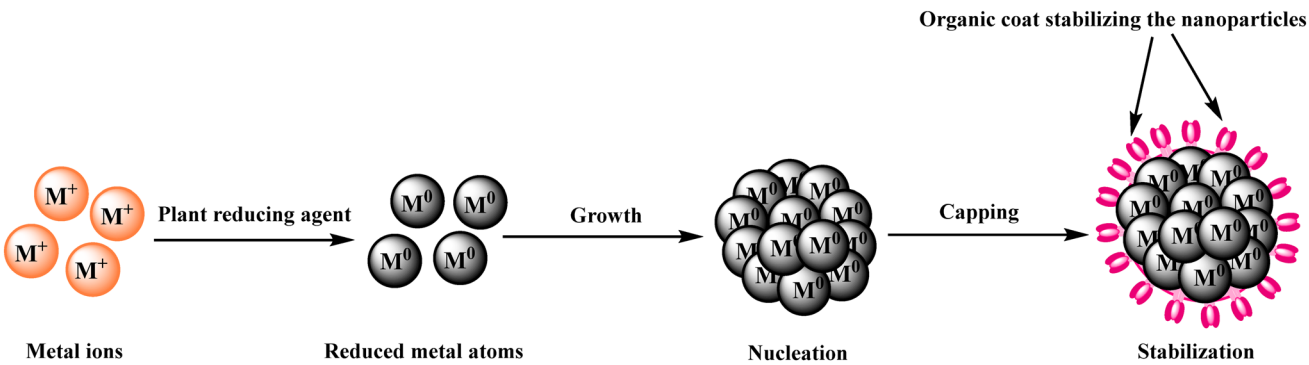

Fig. 1 Schematic illustration of nanoparticles synthesis using the plant extract

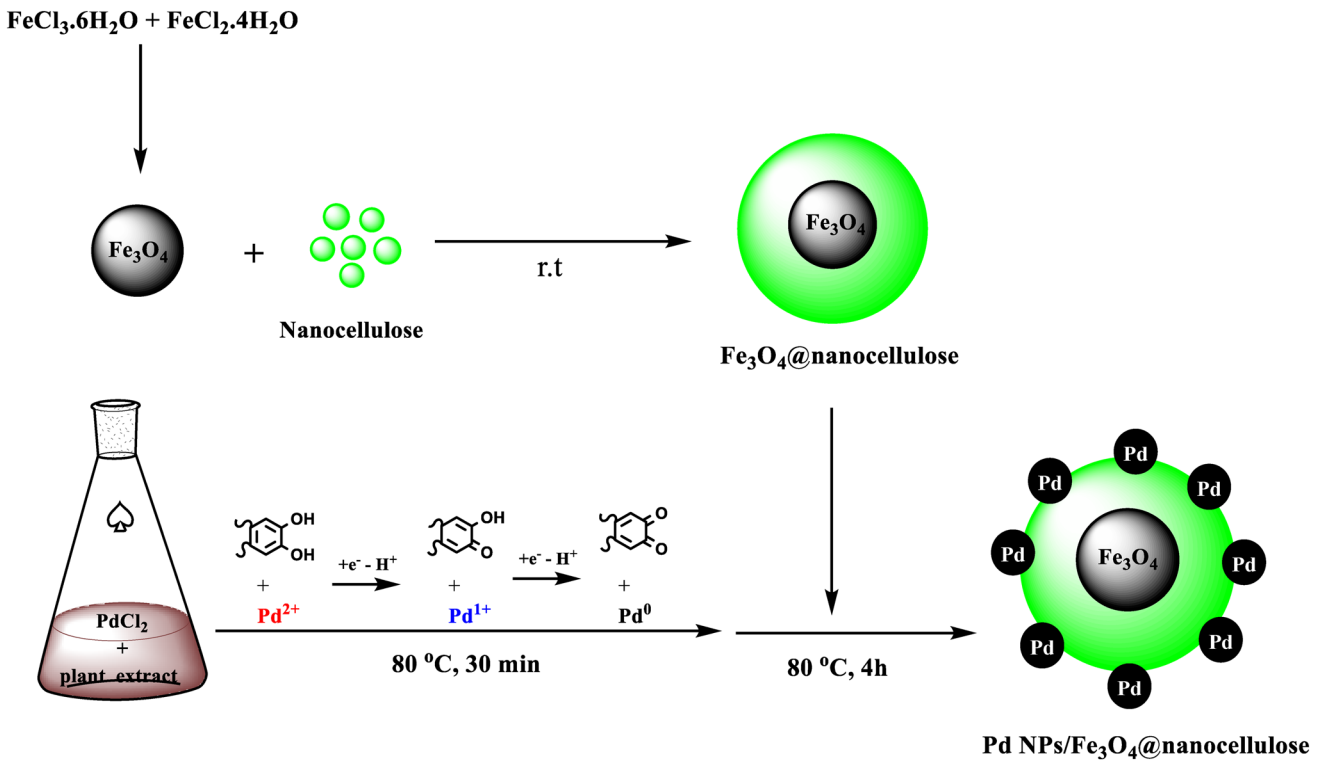

Fig. 2 Schematic illustration for the green synthesis of Pd NPs/Fe_3O_4@nanocellulose catalyst

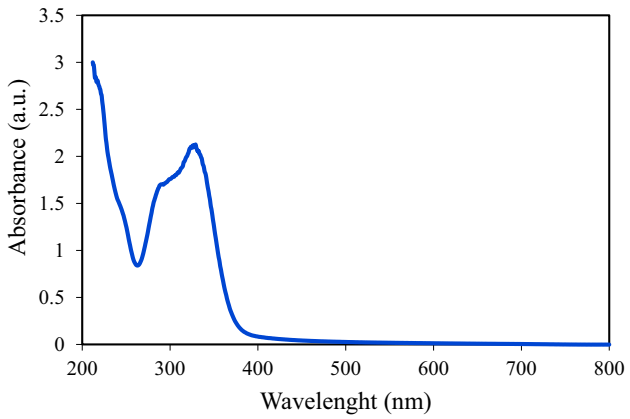

Fig. 3 UV–Vis spectrum of the *Chelidonium majus* extract

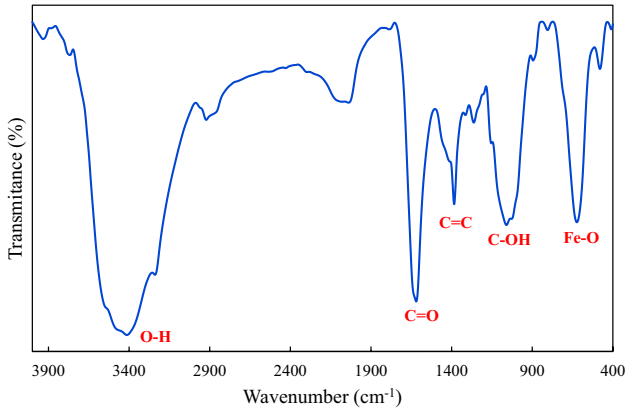

Fig. 4 FT-IR spectrum of the green synthesized Pd NPs/Fe_3O_4@nanocellulose

2.1 Preparation of *Chelidonium majus* (Greater Celandine) Extract

10 g of dried powder of *Chelidonium majus* roots were mixed to 150 mL of distilled water at 70 °C for 45 min. The mixture was then cooled down to room temperature. The extract was collected by centrifugation at 6500 rpm, followed by filtration. The sample was kept at refrigerator for further use [32].

2.2 Preparation of Fe_3O_4@nanocellulose

First, 1gr of PEG-2000 and 9.0 g of NaOH were added into 90 mL of DI water to prepare the aqueous solution of PEG/NaOH. Then, 2.0 g of nanocellulose was added to the solution and stirred for 3 h at room temperature to obtain a white suspension. The suspension was then cooled down to -15 °C and kept at that temperature overnight (12 h) until it became a solid frozen mass. The frozen solid was stirred

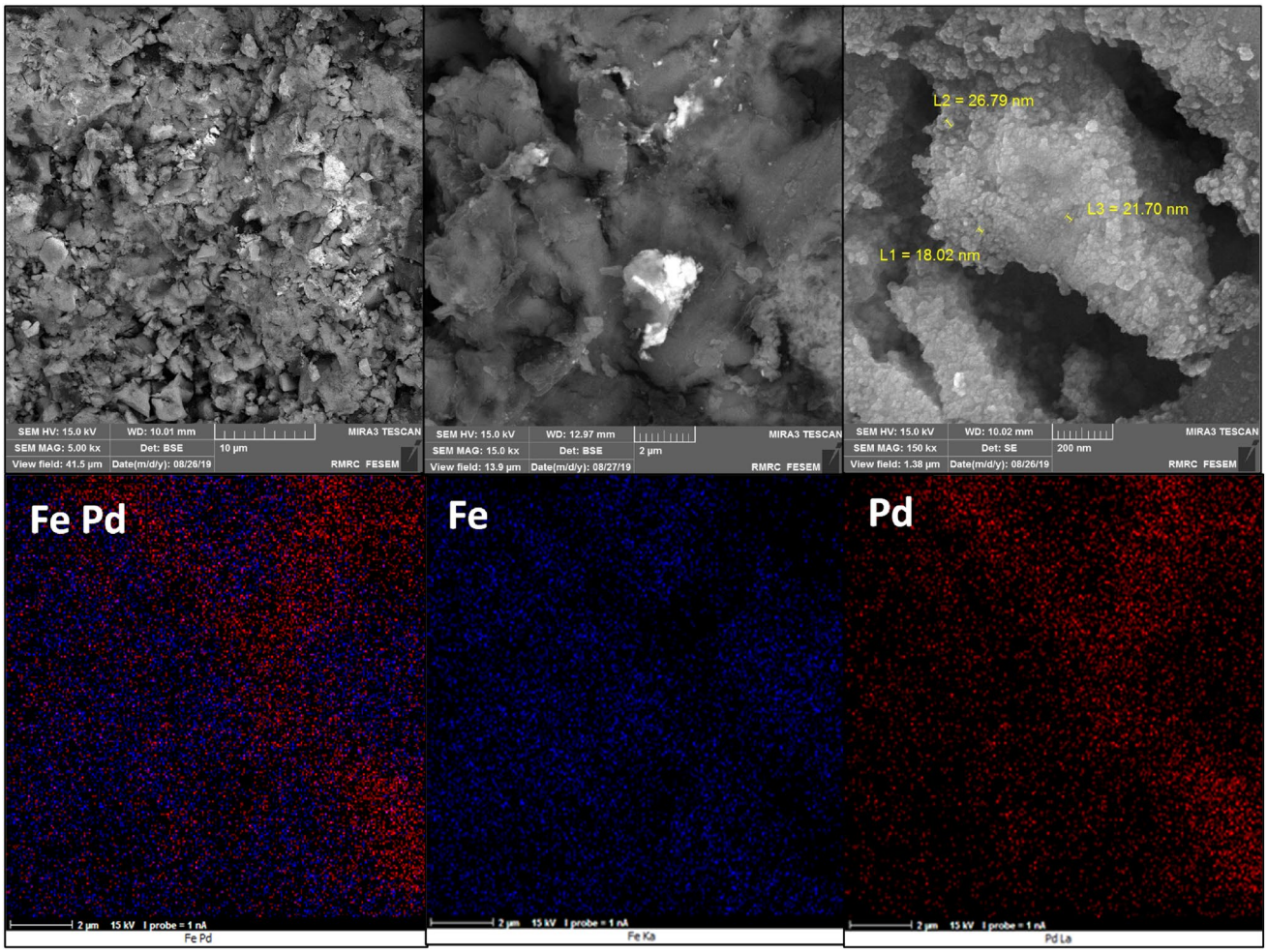

Fig. 5 FE-SEM images and elemental mapping analysis for the Pd NPs/Fe_3O_4@nanocellulose catalyst

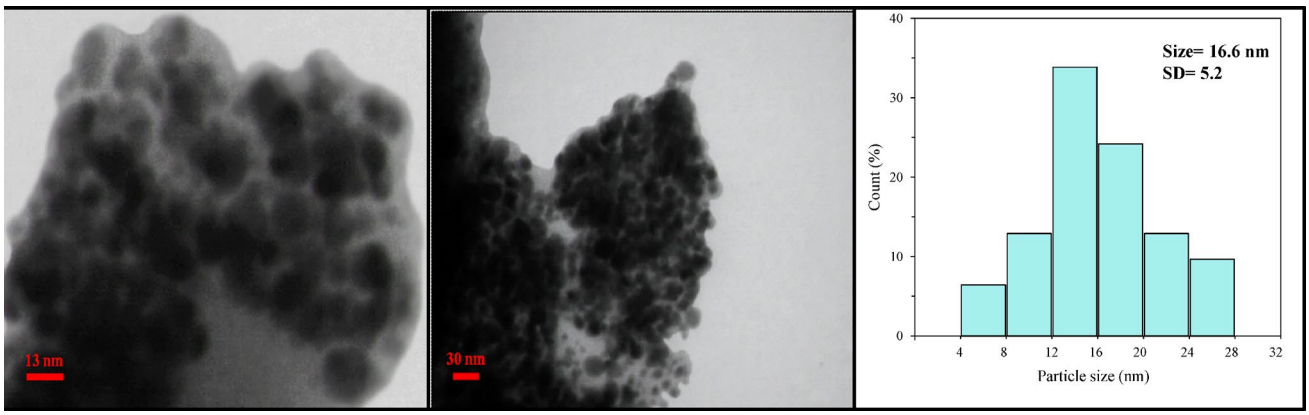

Fig. 6 TEM images and histogram of particle size distribution of the Pd NPs/Fe_3O_4@nanocellulose catalyst

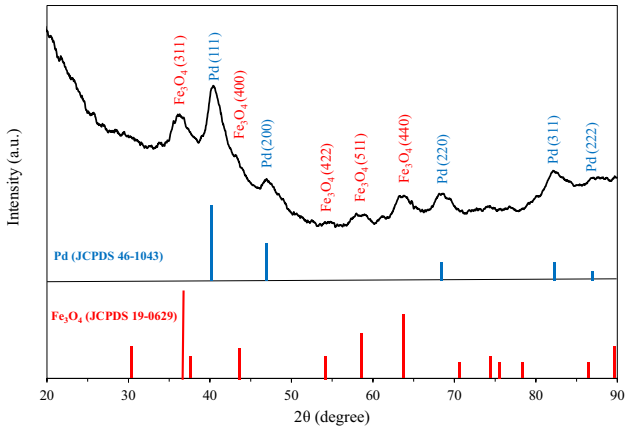

Fig. 7 XRD pattern of the Pd NPs/Fe_3O_4@nanocellulose catalyst

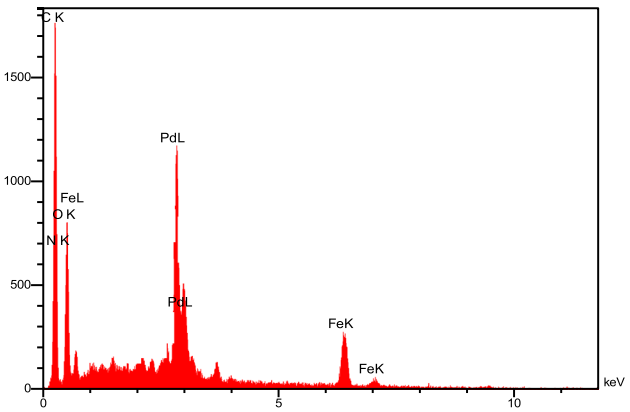

Fig. 8 EDS spectrum of the Pd NPs/Fe_3O_4@nanocellulose catalyst

Table 1 Atomic and weight ratios of the Pd NPs/Fe_3O_4@nanocellulose catalyst

Entry	Element	Line	Weight%	Atom%
1	Carbon	K	42.72	60.75
2	Oxygen	K	26.53	28.32
3	Iron	K	8.96	5.84
4	Palladium	L	17.62	2.83
5	Nitrogen	K	4.17	5.09

under strong stirrer at room temperature. At the end, a homogeneous cellulose solution was achieved [33].

2.3 Green Synthesis of Pd NPs/Fe_3O_4@nanocellulose

In order to synthesis the magnetic nanocellulose catalyst modified by Pd NPs, 0.06 g of $PdCl_2$ was first added to three 50 mL beakers. Thereafter, 10 mL of DI water and 6 drops of the HCl (37%) were added to the beakers. To fully disperse

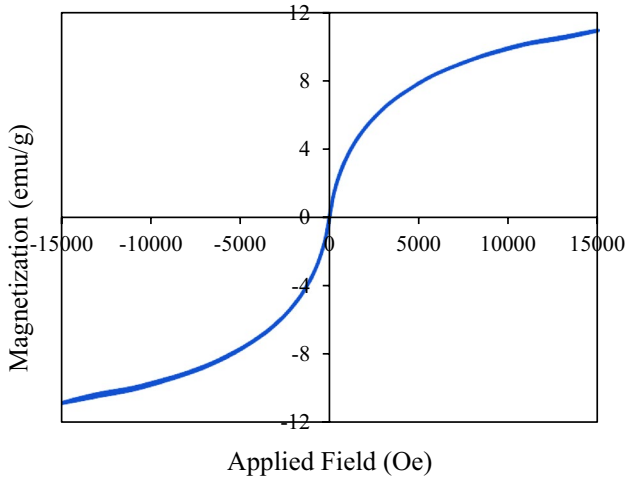

Fig. 9 Magnetization curve for the Pd NPs/Fe_3O_4@nanocellulose catalyst

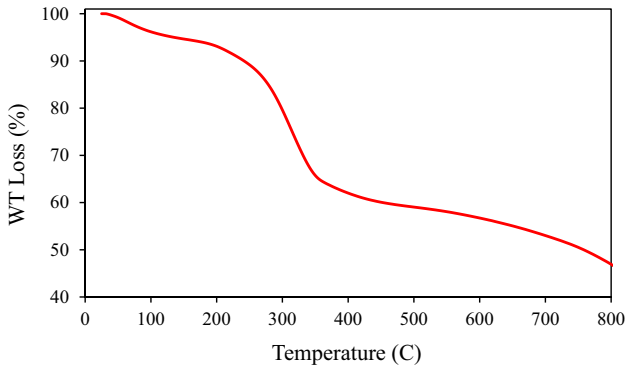

Fig. 10 TGA data measured for the Pd NPs/Fe_3O_4@nanocellulose catalyst

the Pd NPs in the solution, it was sonicated for 30 min at 50 °C. The prepared solution was immediately transferred to the other beaker containing 40 mL of *Chelidonium majus* extract, and stirred at 80 °C. After 30 min, 1 g of magnetic nanocellulose substrate was added to the mixture. The mixture was then refluxed and stirred at 80 °C for 4 h, followed by cooling down to room temperature. Finally, the synthesized catalyst was centrifuged at 6000 rpm for 20 min, rinsed with DI water, and dried at room temperature.

2.4 Catalytic Reduction of Cr(VI) to Cr(III)

The catalytic reduction of Cr(VI) to Cr(III) by formic acid was performed to evaluate the catalytic efficaciously and recyclable of Pd NP-immobilized Fe_3O_4@nanocellulose. 10.0 mg of the Pd NPs/Fe_3O_4@nanocellulose was added into a $K_2Cr_2O_7$ solution (3.4 mM, 25 mL) and formic acid (85%, 1 mL) at 50 °C under mild magnetic stirring. The

degradation process was monitored by the decay of the specific absorption band of Cr(VI) at 352 nm via UV–Vis spectroscopy. Afterwards, the Pd NPs/Fe_3O_4@nanocellulose was collected by an external magnet, rinsed with DI water, and blotted via a filter paper. The synthesized Pd NPs/Fe_3O_4@nanocellulose was reused for successive cycles of catalytic reaction.

2.5 General Procedure for the Reduction of MO, MB, RhB and CR at Room Temperature

The catalytic activity of the Pd NPs/Fe_3O_4@nanocellulose catalyst was evaluated via reduction of aqueous solution of MO, MB, RhB and CR. In the typical method, 25 mL of a newly solution of $NaBH_4$ (5.3×10^{-3} M) was added into a beaker. 25 mL of the prepared dye solution with 10 ppm concentration was then added. The mixture was mixed for 2 min at room temperature. Then, 10 mg of catalyst was added and the mixture was stirred continuously until the color of the solution disappeared. The reduction was followed via UV–Vis absorption spectrophotometer. At the end of the reaction, the catalyst was collected by an external magnet, washed several times with DI water, and dried for further use.

3 Results and Discussion

3.1 Physical and Microstructural Characterizations

In this paper, the Pd NPs/Fe_3O_4@nanocellulose catalyst was synthesized without addition of any chemical reducing agent in two steps. At the first step, Fe_3O_4@nanocellulose was prepared. Thereafter, palladium precursor was reduced to palladium nanoparticles using the *Chelidonium majus* extract, immobilized onto the substrate (Fe_3O_4@nanocellulose). Figure 2, displays the schematic of the green synthesis mechanism for fabrication of the Pd NPs/Fe_3O_4@nanocellulose catalyst. UV–Vis spectrum of the extract, shown in Fig. 3, reveals bands at 285 nm (band I) and 330 nm (band II) which are related to the cinnamoyl and benzoyl systems of phenolics compounds. Therefore, the obtained result proves the presence of phenolics, related to the $\pi \rightarrow \pi^*$ transitions as reported in literatures [34, 35].

FT-IR spectrum of the Pd NPs/Fe_3O_4@nanocellulose is presented in Fig. 4. The spectrum of cellulose has shown the absorption bands at 3413 cm^{-1} and 3239 cm^{-1} in accordance with the stretching vibrations of OH groups and the absorption band at 1619 cm^{-1} demonstrating the stretching vibrations of C=O bonds related to functional groups available in flavonoids and other phenolic components in the roots plant of *Chelidonium majus* [36] that can represent bio reduction of metal ions [34, 35]. Stretching vibrations of Fe–O groups at 623 cm^{-1} are also detected, indicating that the magnetic Fe_3O_4 nanoparticles are coated by nanocellulose. In addition, the absorption bands at 1060 cm^{-1} and 1384 cm^{-1} illustrate the presence of the chemical functional groups, C–OH vibrations and C=C aromatic ring, respectively [37, 38].

Figure 5 shows morphology of Pd NPs/Fe_3O_4@nanocellulose catalyst studied by FE-SEM. As can be seen, spherical

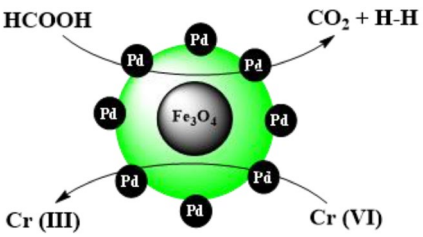

1) $HCOOH \longrightarrow CO_2 + H_2$

2) $Cr_2O_7^{2-} + 8H^+ + 3H_2 \longrightarrow 2Cr^{3+} + 7H_2O$

Fig. 12 Proposed mechanism for reduction of Cr(VI) to Cr(III) on the Pd NPs/Fe_3O_4@nanocellulose catalyst in the presence of formic acid

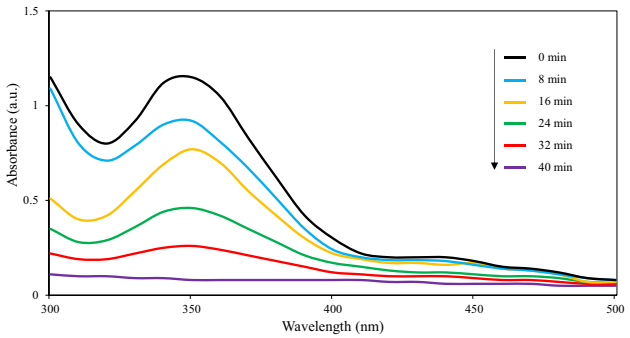

Fig. 11 UV–Vis spectra for Cr(VI) reduction on the Pd NPs/Fe_3O_4@nanocellulose catalyst in the presence of formic acid (1.0 mL)

Table 2 Optimization conditions for reduction of Cr(VI) using the Pd NPs/Fe_3O_4@nanocellulose catalyst at 50 °C

Entry	Catalyst (mg)	Formic acid (mL)	Time
1	–	1.0	3.30 h[a]
2	Fe_3O_4@nanocellulose (10 mg)	1.0	3.30 h[b]
3	Pd NPs/Fe_3O_4@nanocellulose (5 mg)	1.0	1.30 h
4	Pd NPs/Fe_3O_4@nanocellulose (7 mg)	1.0	55 min
5	Pd NPs/Fe_3O_4@nanocellulose (10 mg)	1.0	40 min

[a]No reaction

[b]Not complete

Table 3 Comparison of the results of this work with other literatures methods in the reduction of the Cr(VI)

Initial Cr(VI) conc. (ppm)	Catalyst	Catalyst loading (g/L)	Temperature (°C)	Sacrificial reagent	Time	References
10	$rGO-Sm_2MoO_6-TiO_2$	5	–	Sulfuric acid	70 min	[40]
20	$UV/ZnO–TiO_2$	1	–	–	120 min	[41]
20	2/5 wt% SO_4^{2-}/TiO_2	0.6	–	EDTA	180 min	[42]
30	ZSM-5 zeolite	0.4	20	Oxalate	24 h	[43]
Pt/Cr = 1/710	2 wt% Pt@MIL-101	–	50	Formic acid	60 min	[44]
Pd/Cr = 1/710	2 wt% Pd@MIL-101	–	50	Formic acid	210 min	[44]
4	TiO_2/MWCNTs	0.2	–	Potassium sulfate	6 h	[45]
5	TiO_2	5	–	Hydrogen peroxide	60 min	[46]
30	ZnO/kaolin	1	–	Citric acid	120 min	[47]
260	Pd/C	2	50	Formic acid	70 min	[48]
354	Pd NPs/Fe_3O_4@nanocellulose	0.4	50	Formic acid	40 min	This work

particles with diameters in the range of 18-27 nm were deposited on the Fe_3O_4@nanocellulose support, proving a perfect combination of the Pd NPs and the Fe_3O_4@nanocellulose support.

The TEM micrographs of the synthesized Pd NPs/Fe_3O_4@nanocellulose catalyst are presented in Fig. 6. The TEM study clarified that the average particle size of the Pd NPs/Fe_3O_4@nanocellulose catalyst is 16.6 ± 5.2 nm which is in agreement with the FE-SEM results. The Pd NPs/Fe_3O_4@nanocellulose catalyst possesses Fe_3O_4 and Pd NPs with spherical morphology incorporated discretely with cellulose. The presence of nanocellulose reduces the level of Fe_3O_4 and Pd NPs agglomeration during the reaction, providing facile magnetic separation [39].

The XRD pattern of the Pd NPs/Fe_3O_4@nanocellulose is shown in Fig. 7. The characteristic peaks for the Fe_3O_4 phase were detected at $2\theta = 35.55°$, 43.07°, 57.50° and 60.70° corresponding to the crystal planes of (3 1 1), (4 0 0), (4 2 2), (5 1 1), and (4 4 0), respectively. The peaks are quite matched with the cubic spinel structure of pure Fe_3O_4. Other diffraction peaks at $2\theta = 39.89°$, 46.55°, 67.72°, 81.2° and 87.1° corresponding to the Pd crystal planes of (1 1 1), (2 0 0), (2 2 0), (3 1 1), and (2 2 2), respectively reveal the existence of Pd NPs. The diffraction peaks for cellulose phase at 16.45° and 22.18° have been placed in the background level of the diffraction pattern.

The Debye–Scherrer equation ($D = 0.94\lambda/\beta_{1/2}\,\mathrm{Cos}(\theta)$) was also used to estimate the crystallite size of Pd NPs, where D is the average crystallite size (nm), λ is the X-ray source wavelength (nm), $\beta_{1/2}$ is the line broadening half the maximum peak intensity (FWHM; radians), and θ is the Bragg angle. The average crystallite size for the Pd NPs was measured as 5.13 nm using the most intense Pd diffraction peak at $2\theta = 39.89°$, shown in Fig. 7.

The EDS results for the Pd NPs/Fe_3O_4@nanocellulose, presented in Fig. 8 and Table 1, demonstrate that the synthesized catalyst is composed of C, O, Pd, Fe elements without any possible impurities which can be formed during synthesis process. It should be noted that nitrogen normally presents in the FE-SEM chamber. In addition, Table 1 demonstrates the quantitative analysis results containing the weight percentage and atomic percentage of the elements.

Magnetic features of the synthesized Pd NPs/Fe_3O_4@nanocellulose was evaluated using VSM at room temperature with field sweeping from − 15,000 to + 15,000 Oe. Figure 9 shows the characteristic hysteresis loop of the Pd NPs/Fe_3O_4@nanocellulose with saturation magnetization of 10.93 emu/g, demonstrating the magnetic nature of the synthesized catalyst. Therefore, after completion of the reaction, catalyst could easily be separated by using an external magnet from the reaction medium.

Thermal behavior of the Pd NPs/Fe_3O_4@nanocellulose catalyst analyzed via TGA is shown in Fig. 10. The sample experiences a little weight loss at the beginning of temperature ascent. The weight loss observed over 150 °C is due to removal of the adsorbed water and the residual organics from the Pd NPs/Fe_3O_4@nanocellulose catalyst. The main weight loss which occurs at 250–350 °C is basically due to thermal decomposition of the cellulose (thermal decomposition temperature is in the range of 260–340 °C). Furthermore, at this step, the weight loss of the cellulose is clearly higher than that of the Pd NPs/Fe_3O_4@nanocellulose catalyst.

3.2 Activity of the Pd NPs/Fe_3O_4@nanocellulose for Reduction of Cr(VI)

To explore the catalytic operation of the synthesized Pd NPs/Fe_3O_4@nanocellulose catalyst, toxic Cr(VI) was reduced in the presence of formic acid. The $K_2Cr_2O_7$

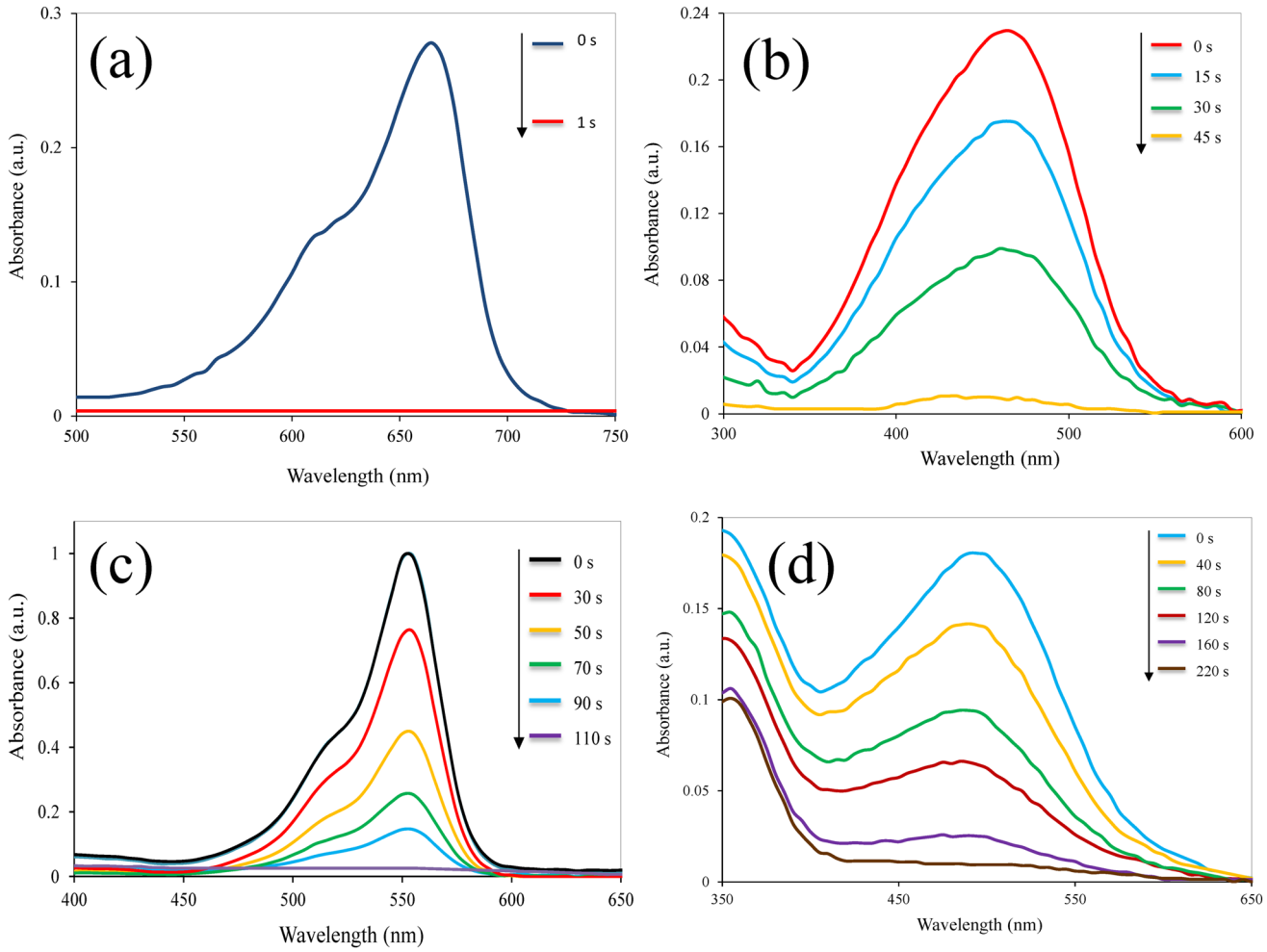

Fig. 13 Time related UV–Vis spectral alteration for the reaction mixture of **a** MB, **b** MO, **c** RhB and **d** CR in the presence of $NaBH_4$ catalyzed by the Pd NPs/Fe_3O_4@nanocellulose catalyst

Table 4 The effect of Pd NPs/Fe_3O_4@nanocellulose loadings on reduction of MB, MO, RhB and CR

Entry	Dye (M)	Catalyst (mg)	Time
1	MB (3.1×10^{-5})	3.0 mg	15 s
2		5.0 mg	Immediately
3	MO (3.0×10^{-5})	5.0 mg	90 s
4		7.0 mg	60 s
5		10.0 mg	45 s
6	RhB (2.09×10^{-5})	5.0 mg	240 s
7		7.0 mg	150 s
8		10.0 mg	110 s
9	CR (1.44×10^{-5})	5.0 mg	300 s
10		7.0 mg	260 s
11		10.0 mg	220 s

Reaction conditions: Dyes (25 mL), $NaBH_4$ (5.3×10^{-3} M, 25 mL), room temperature. Reduction reactions were examined by UV–Vis

was chosen as one of the indicative Cr(VI) compounds. The maximum absorbance peak for Cr(VI) is around ~ 250–500 nm which is originated by transition of metal Cr(VI) and ligand (oxygen). By adding the Pd NPs/Fe_3O_4@nanocellulose to Cr(VI) and also using HCOOH as a reducing agent, the color of the solution gradually alters from yellow to colorless. The absorption peak at 352 nm slowly decreases and disappears within 40 min. The exact time of reduction process was monitored by UV–Vis spectroscopy, shown in Fig. 11. After addition of the Pd NPs/Fe_3O_4@nanocellulose to a mixture of Cr(VI) and HCOOH, formic acid is first adsorbed onto the catalyst surface and then dehydrogenated into CO_2 and H_2 (Eq. (1), Fig. 12). The produced H_2 is adsorbed on active sites of Pd NPs/Fe_3O_4@nanocellulose which acts as reducing agent for reduction Cr(VI) to Cr(III) (Eq. (2), Fig. 12). It should be noted that formic acid is considered as a hydrogen donor for reduction of Cr(VI). The catalytic performance of the Pd NPs/Fe_3O_4@nanocellulose catalyst results in formic

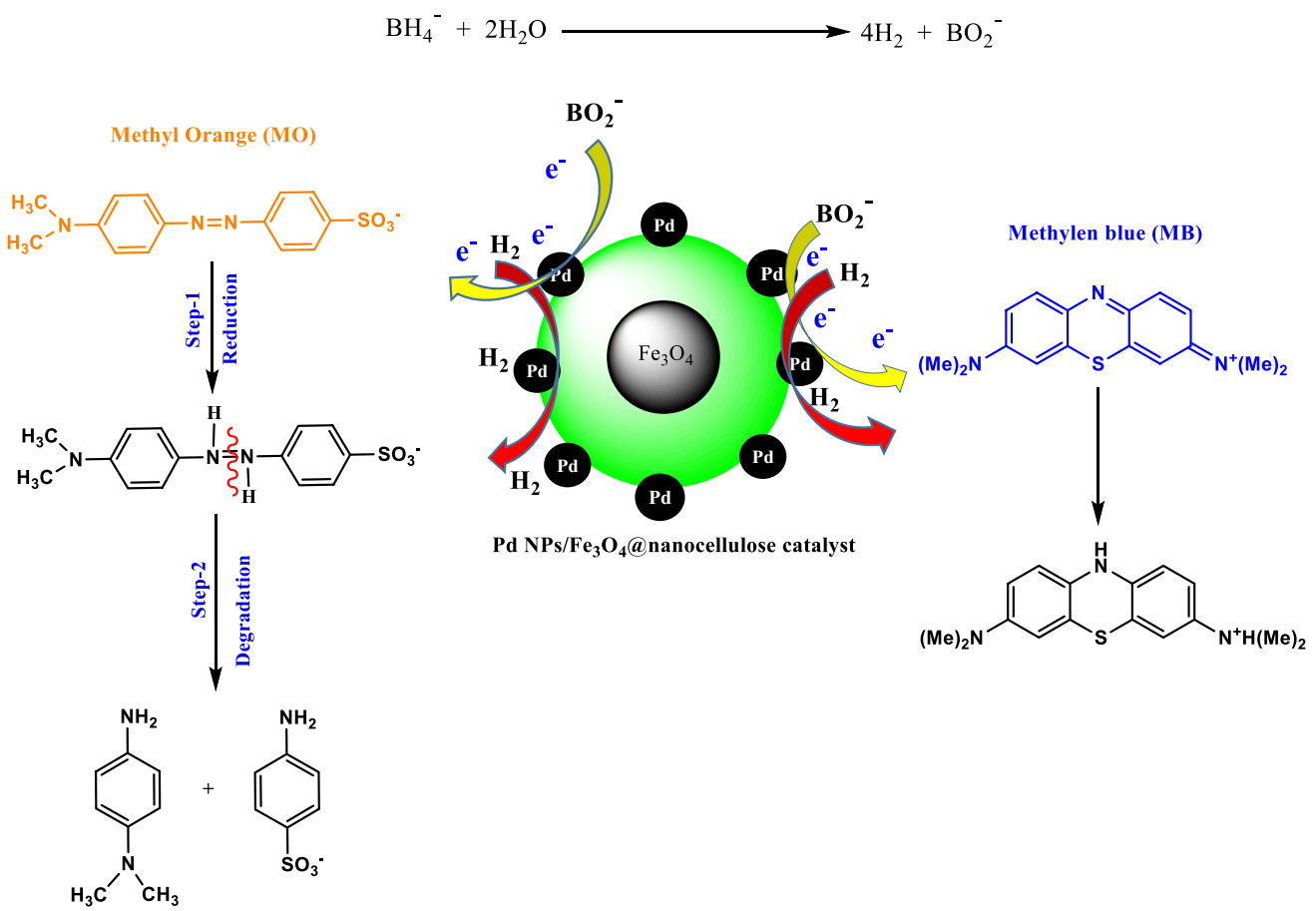

Fig. 14 Proposed mechanism for the reduction of organic dyes (MB and MO) by Pd NPs/Fe_3O_4@nanocellulose catalyst

acid decomposition, leading to hydrogen gas production. The produced hydrogen gas is used as the hydrogen source for the Cr(VI) reduction reaction. Figure 12, illustrates the schematic of the proposed mechanism for reduction of Cr(VI) to Cr(III) on the Pd NPs/Fe_3O_4@nanocellulose catalyst in the presence of formic acid. The formation of Cr(III) is confirmed by adding an excess of NaOH (1.0 M) solution, where the color of solution changes from colorless to green. Variation of catalyst loading also plays an important role in Cr(VI) reduction reaction time, investigated in Table 2. As can be seen, the reaction does not happen without the presence of catalyst, even with the presence of formic acid. Also, the reaction is not fully performed using the Fe_3O_4@nanocellulose substrate in the presence of formic acid. After optimizing the amount of Pd NPs/Fe_3O_4@nanocellulose catalyst with values of 5, 7 and 10 mg to perform the reduction of Cr(VI), it was concluded that 10 mg of catalyst results in shortest possible time to end the reaction. A comparative study between the synthesized Pd NPs/Fe_3O_4@nanocellulose catalyst and other catalysts used in the literature is presented in Table 3. The results clearly demonstrate higher catalytic performance of the synthesized Pd NPs/Fe_3O_4@nanocellulose catalyst compared to those reported for the other catalysts.

3.3 Activity of the Pd NPs/Fe_3O_4@nanocellulose for Reduction of MO, MB, RhB and CR

Catalytic reduction of MO, MB, RhB, and CR dyes under influence of $NaBH_4$ was also investigated to evaluate the efficiency of the synthesized Pd NPs/Fe_3O_4@nanocellulose catalyst. The reactions progress was monitored by UV–Vis spectroscopy. As shown in the UV–Vis spectra in Fig. 13, MB (a), MO (b), RhB (c) and CR (d) in water solution exhibit peaks at 663, 465, 554 and 493 nm, respectively. According to the results, after the addition of $NaBH_4$ aqueous solution and 5.0 mg of the catalyst, the complete reduction of MB occurred immediately, while reduction of MO, RhB and CR were completed within 45, 110 and 220 s, respectively by adding of 10.0 mg of the catalyst. As shown in Table 4, by optimizing catalyst loading and minimizing molar ratio of $NaBH_4$ on MO, MB, RhB and CR, reactions were completed in different times.

Table 5 Comparison between the other catalysts reported in the literature and this work in reduction of MB, MO, RhB and CR

Dye conc. (M)	Catalyst	Catalyst value	$NaBH_4$ conc. (M)	Time	References
MB (3.1×10^{-5})	Ag/HZSM-5	5 mg	(5.3×10^{-3})	94 s	[50]
MB (3.0×10^{-5})	12.5 Cu@SBA-15	–	(2.5×10^{-2})	8 min	[51]
MB (1.0×10^{-5})	Fe_3O_4@C@Au	5 mg	(5.0×10^{-3})	10 min	[52]
MB (3.0×10^{-5})	Cu/Al_2O_3 NPs	10 mg	(5.0×10^{-3})	33 s	[53]
MB (3.1×10^{-5})	Pd NPs/Fe_3O_4@nanocellulose	5 mg	(5.3×10^{-3})	Immediately	This work
MO (3×10^{-5})	Natrolite zeolite/Pd	20 mg	(5.3×10^{-3})	2 min	[54]
MO (15×10^{-5})	CuSbOS	10 mg	(10.0×10^{-1})	40 min	[55]
MO (3×10^{-5})	1% Co-ZW/UV–Vis	–	–	120 min	[56]
MO (3×10^{-5})	C_{60}-AuNPs-TiO_2/halogen lamp	20 mg	–	160 min	[57]
MO (3.0×10^{-5})	Pd NPs/Fe_3O_4@nanocellulose	10 mg	(5.3×10^{-3})	45 s	This work
RhB (1×10^{-5})	Ag-Fe_3O_4	20 mg	(5.0×10^{-2})	15 min	[58]
RhB (1×10^{-4})	CuSbOS	10 mg	(10.0×10^{-1})	12 min	[55]
RhB (1×10^{-5})	1% Co-ZW/UV–Vis	–	–	120 min	[56]
RhB (1×10^{-5})	$Bi_2O_2CO_3$/visible-light	100 mg	–	90 min	[59]
RhB (2.09×10^{-5})	Pd NPs/Fe_3O_4@nanocellulose	10 mg	(5.3×10^{-3})	110 s	This work
CR (1.0×10^{-5})	DLP -AuNPs	100 µL	(1.0×10^{-3})	10 min	[60]
CR (2.0×10^{-5})	Pd/ZnO- UV–Vis	20 mg	–	90 min	[61]
CR (2.0×10^{-5})	ZnO/UV–Vis	20 mg	–	210 min	[61]
CR (2.0×10^{-5})	Ag-enterapped-hydrogel	10 mg	(10×10^{-3})	40 min	[62]
CR (1.44×10^{-5})	Pd NPs/Fe_3O_4@nanocellulose	10 mg	(5.3×10^{-3})	220 s	This work

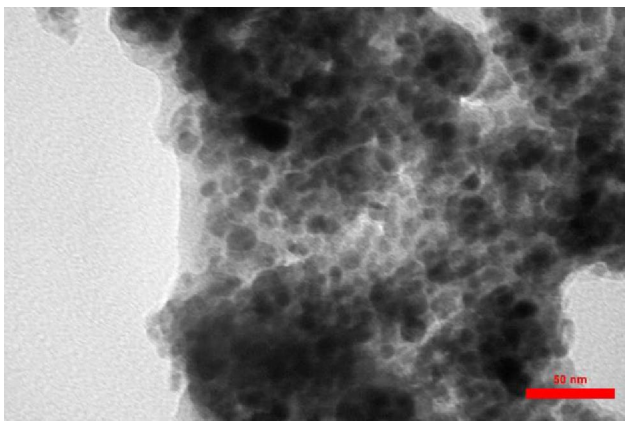

Fig. 15 The TEM image of the recycled Pd NPs/Fe_3O_4@nanocellulose catalyst

According to the results for reduction of organic dyes, it is assumed that first MB, MO, RhB or CR is adsorbed onto the surface of Pd NPs/Fe_3O_4@nanocellulose catalyst to create metal hydride as a hydrogen mediator. Thereafter, H_2 gas and BO_2^- are produced by hydrolysis of borohydride ions. The Pd NPs/Fe_3O_4@nanocellulose as a redox catalyst facilitates electron transfer between donor species BO_2^- and acceptor molecules MB, MO, RhB or CR (Fig. 14) [49].

In this research, it was observed that not only the degradation of organic dyes cannot occur without $NaBH_4$, but also the absorbance of dyes media remains unchanged for several hours in absence of the catalyst. The results illustrate that the Pd NPs/Fe_3O_4@nanocellulose catalyst leads to a highly efficient reaction completed in a short time compared to other catalysts. Table 5 displays a comparison between the synthesized Pd NPs/Fe_3O_4@nanocellulose catalyst and the other catalysts studied in the literature for reduction of dyes.

3.4 Catalyst Recyclability

The recyclability of the heterogeneous catalysts is one of the most important advantages of them for industrial applications. The synthesized Pd NPs/Fe_3O_4@nanocellulose catalyst could simply be separated from the reaction container by several ways such as centrifugation or using an external magnet. The separated catalyst can be then washed several times with DI water, dried and used for next reactions. This procedure was used in four sequential reactions for 100% reduction of MO. The TEM analysis, shown in Fig. 15, implies upon the stability of the Pd NPs/Fe_3O_4@nanocellulose catalyst after the forth recycle, illustrating no significant change in the catalyst structure. The Pd NPs/Fe_3O_4@nanocellulose catalyst was also applied for four cycles of 100% reduction of CR and Cr(VI). The measured times required for those reduction reaction were almost the same as their first cycle.

4 Conclusions

In this study, a green, facile, economic and efficient method was demonstrated for the synthesis of Pd NPs/Fe_3O_4@nanocellulose catalyst via *Chelidonium majus* plant extract as an eco-friendly reducing agent and cellulose as a natural support. The results showed an excellent improvement in reduction reaction to eliminate toxic and dangerous Cr(VI), MB, MO, RhB and CR compounds in the aqueous medium. Furthermore, the catalyst was easily separated by an external magnet from the reaction mixture and recovered for four times without significant decrease in catalytic activity. Hence, this stable synthesis technique can be carried out for a wide range of applications.

References

1. S. Langård, *Biological and Environmental Aspects of Chromium* (Elsevier, Amestrdam, 2013)
2. P.A. Lay, A. Levina, J. Am. Chem. Soc. **120**(27), 6704–6714 (1998)
3. A. Levina, R. Codd, C.T. Dillon, P.A. Lay, Prog. Inorg. Chem. **51**, 145–250 (2003)
4. F.N. Acer, E. Malkoc, Bioresour. Technol. **94**, 13–15 (2004)
5. P. Kajitvichyanukul, J.A. Pattarchai, S. Pongpom, Sci. Technol. Adv. Mater. **6**, 352–358 (2005)
6. S.K. Shrivastava, V.K. Gupta, D. Mohan, J. Environ. Model. Assess. **1**, 281–290 (1996)
7. P. Suksabyea, A. Nakajimab, P. Thiravetyan, J. Hazard. Mater. **161**, 1103–1108 (2009)
8. J.B. Vincent, Sports Med. **33**, 213–300 (2003)
9. A. Hassani, L. Alidokht, A.R. Khataee, S. Karaca, J. Taiwan Inst. Chem. Eng. **45**, 1597–1607 (2014)
10. M.A. Omole, V.A. Okello, V. Lee, L. Zhou, O.A. Sadik, ACS Catal. **1**, 139–146 (2011)
11. D. Park, Y.S. Yun, J.M. Park, Environ. Sci. Technol. **38**, 4860–4864 (2004)
12. R.R. Patterson, S. Fendorf, Environ. Sci. Technol. **31**, 2039–2044 (1997)
13. N. Daneshvar, D. Salari, S. Aber, J. Hazard. Mater. **94**, 49–61 (2002)
14. A. Dandapat, D. Jana, G. De, Appl. Catal. **396**, 34–39 (2011)
15. N. Farahbakhsh, P.S. Roodposhti, A. Ayoub, R.A. Venditti, J.S. Jur, J. Appl. Polym. Sci. **132**(17), 41857 (2015)
16. C.A. de Assis, M.C. Iglesias, M. Bilodeau, D. Johnson, R. Phillips, M.S. Peresin, E.M. Bilek, O.J. Rojas, R.A. Venditti, R. Gonzalez, Biofuels. Bioprod. Biorefin. **12**(2), 251–264 (2018)
17. A. Mirosanloo, D. Zareyee, M.A. Khalilzadeh, Appl. Organomet. Chem. **32**(12), e4546 (2018)
18. Y. Jiao, C. Wan, W. Bao, H. Gao, D. Liang, J. Li, Carbohydr. Polym. **189**, 371–378 (2018)
19. P. Sharma, S. Rana, K.C. Barick, C. Kumar, H.G. Salunke, P.A. Hassan, New J. Chem. **38**(11), 5500–5508 (2014)
20. Y.M. Huh, Y.W. Jun, H.T. Song, S. Kim, J.S. Choi, J.H. Lee, S. Yoon, K.S. Kim, J.S. Shin, J.S. Suh, J. Cheon, J. Am. Chem. Soc. **127**(35), 12387–12391 (2005)
21. M. Maleki, S.M. Baghbanian, M. Tajbakhsh, J. Iran. Chem. Soc. **15**(2), 359–368 (2018)
22. T.A. GadAllah, S. Kato, S. Satokawa, T. Kojima, Solid State Sci. **9**(8), 737–743 (2007)
23. R. Hosseinzadeh, M. Mavvaji, M. Tajbakhsh, Z. Lasemi, N. Aghili, Org. Prep. Proced. Int. **52**(2), 99–109 (2020)
24. S. Tajik, H. Beitollahi, M.R. Aflatoonian, B. Mohtat, B. Aflatoonian, I.S. Shoaie, M.A. Khalilzadeh, M. Ziasistani, K. Zhang, H.W. Jang, M. Shokouhimehr, RSC Adv. **10**(26), 15171–15178 (2020)
25. A. Abri, M. Tajbakhsh, A. Sadeghi, Water Supply **19**(1), 40–51 (2019)
26. D. Goia, C.E. Matijevi, Colloids Surf. A Physicochem. Eng. Asp. **146**, 139–152 (1999)
27. S.L. Smitha, K.M. Nissamudeen, D. Philip, Spectrochim. Acta A Mol. Biomol. Spectrosc. **71**, 186–190 (2008)
28. S. Naraginti, Y. Li, J. Photochem, Photobiol. B Biol. **170**, 225–234 (2017)
29. C.J. Kirubaharan, D. Kalpana, Y.S. Lee, Ind. Eng. Chem. Res. **51**, 7441–7446 (2012)
30. S. Iravani, Green Chem. **13**, 2638–2650 (2011)
31. M.A. Khalilzadeh, S. Tajik, H. Beitollahi, R.A. Venditti, Ind. Eng. Chem. Res. **59**(10), 4219–4228 (2020)
32. F. Khaleghi, L.B. Din, F.R. Charati, W.A. Yaacob, M.A. Khalilzadeh, B. Skelton, M. Makha, Phytochem. Let. **4**(3), 254–258 (2011)
33. E. Kalantari, M.A. Khalilzadeh, D. Zareyee, M. Shokouhimehr, J. Mol. Struct. **1218**, 128488 (2020)
34. R. Dai, J. Chen, J. Lin, S. Xia, S. Chen, Y. Deng, J. Hazard. Mater. **170**(1), 141–143 (2009)
35. B. Naik, S. Hazra, P. Muktesh, V.S. Prasad, N.N. Ghosh, Sci. Adv. Mater. **3**, 1025–1030 (2011)
36. S. Zavoi, F. Fetia, F. Ranga, R.M. Pop, A. Baciu, C. Socaciu, Not. Bot. Hortic Agrobot. **39**(2), 82–89 (2011)
37. S.H. Adyani, E. Soleimani, J. Hydrog. Energy **44**, 2711–2730 (2019)
38. S. Seyednejhad, M.A. Khalilzadeh, D. Zareyee, H. Sadeghifar, R.A. Venditti, Cellulose **26**, 5015–5031 (2019)
39. A. Alizadeh, M.A. Khalilzadehb, E. Alipour, D. Zareyee, Comb. Chem. High T SCR. **23** (2020). In press
40. A. Raja, P. Rajasekaran, K. Selvakumar, M. Arivanandhan, S. Asath Bahadur, M. Swaminathan, ACS Omega **5**(12), 6414–6422 (2020)
41. M. Naimi-Joubani, M. Shirzad-Siboni, J.K. Yang, M. Gholami, M. Farzadkia, J. Ind. Eng. Chem. **22**, 317–323 (2015)
42. P. Mohapatra, S.K. Samantaray, K. Parida, J. Photochem. Photobiol., A **170**(2), 189–194 (2005)
43. D. Shao, X. Wang, Q. Fan, Microporous Mesoporous Mater. **117**, 243–248 (2009)
44. M. Yadav, Q. Xu, Chem. Commun. **49**, 3327–3329 (2013)
45. X. Tan, M. Fang, X. Wang, J. Nanosci. Nanotechnol. **8**(11), 5624–5631 (2008)
46. M.F. Ghorab, R. Djellabi, R. Messadi, in e3s Web of Conferences. EDP Sciences,↑1, 25008 (2013)
47. M. Shirzad-Siboni, M. Farrokhi, R. Darvishi Cheshmeh Soltani, A. Khataee, S. Tajassosi, Ind. Eng. Chem. Res. **53**(3), 1079–1087 (2014)
48. D.N. Li, F.Q. Shao, J.J. Feng, J. Wei, Q.L. Zhang, A.J. Wang, Mater. Chem. Phys. **205**, 64–71 (2018)
49. S. Carregal-Romero, J. Perez-Juste, P. Herves, L.M. Liz-Marzan, P. Mulvaney, Langmuir **26**(2), 1271–1277 (2010)
50. M. Tajbakhsh, H. Alinezhad, M. Nasrollahzadeh, T.A. Kamali, J. Alloys Compd. **685**, 258–265 (2016)
51. B.K. Ghosh, S. Hazra, B. Naik, N.N. Ghosh, Powder Technol. **269**, 371–378 (2015)
52. Z. Gan, A. Zhao, M. Zhang, W. Tao, H. Guo, Q. Gao, R. Mao, E. Liu, Dalton Trans. **42**, 8597–8605 (2013)
53. M. Nasrollahzadeh, Z. Issaabadi, S.M. Sajadi, Compos. B Eng. **166**, 112–119 (2019)

54. A. Hatamifard, M. Nasrollahzadeh, J. Lipkowski, RSC Adv. **5**(111), 91372–91381 (2015)
55. X. Chen, D.H. Kuo, J. Zhang, Q. Lu, J. Lin, J. Mol. Liq. **275**, 204–214 (2019)
56. U. Alam, A. Khan, D. Bahnemann, M. Muneer, J. Environ. Chem. Eng. **6**(4), 4885–4898 (2018)
57. M.T. Islam, H. Jing, T. Yang, E. Zubia, A.G. Goos, R.A. Bernal, J.C. Noveron, J. Environ. Chem. Eng. **6**(4), 3827–3836 (2018)
58. L. Ai, C. Zeng, Q. Wang, Catal. Commun. **14**(1), 68–73 (2011)
59. P. Madhusudan, J. Zhang, B. Cheng, G. Liu, Cryst. Eng. Commun. **15**, 231–240 (2013)
60. C. Umamaheswari, A. Lakshmanan, N.S. Nagarajan, J. Photochem. Photobiol. B Biol. **178**, 33–39 (2018)
61. N. Güy, M. Özacar, Int. J. Hydrog. Energy **41**(44), 20100–20112 (2016)
62. Y. Zheng, A. Wang, J. Mater. Chem. **22**(32), 16552–16559 (2012)